New insights into bisphenol A removal from water applying experimental and theoretical studies

R.A. Konzen[a],*, P.R. Batista[b], L.C. Ducati[b], T.E.A. Souza[a], L.C. Cavalcante[a], C.E. Santos[c], F.J. Bassetti[a], P.C. Rodrigues[a], L.A. Coral[a]

[a]*Academic Department of Chemistry and Biology, Federal University of Technology – Paraná (UTFPR), Campo Comprido, ZIP Code: 81280-340, 5000 Curitiba-PR, Brazil, Tel. +55 41 99136 0667; emails: raquelkonzen1@gmail.com (R.A. Konzen), thaineh.alves@gmail.com (T.E.A. Souza), cavalcanteluan@hotmail.com (L.C. Cavalcante), bassetti@utfpr.edu.br (F.J. Bassetti), paulac@utfpr.edu.br (P.C. Rodrigues), lucilacoral@utfpr.edu.br (L.A. Coral)*
[b]*Department of Fundamental Chemistry, University of São Paulo – São Paulo (USP), Av. Prof. Lineu Prestes, 748, ZIP Code: 05508-000, São Paulo-SP, Brazil, emails: patrick@iq.usp.br (P.R. Batista), ducati@iq.usp.br (L.C. Ducati)*
[c]*Department of Environmental Engineering and Technology, Federal University of Santa Maria (UFSM), Sete de Setembro, ZIP code 98400-000, Frederico Westphalen-RS, Brazil, email: caroline_emiliano@hotmail.com*

ABSTRACT

Bisphenol A (BPA) is used worldwide as a monomer in the production of polycarbonates and epoxy resins. It has been receiving growing attention over the years, as exposure to even low concentrations of this endocrine disruptor is being linked to serious health problems. This study aims to investigate the efficiency of powdered activated carbon (PAC) in removing BPA from water, as well as to apply a computational simulation to understand the behavior of BPA in solution and its interaction with a generic carbonaceous surface. In the adsorption studies, the mass of adsorbent (0.01–0.04 g) and the solution pH (2–12) were varied in order to understand their influence over the adsorption capacity (q_e) of PAC. Pseudo-first-order, pseudo-second-order, and intraparticle diffusion were employed to evaluate kinetic data. Langmuir, Freundlich, Dubinin–Radushkevich, and Redlich–Peterson isotherm models were applied. A theoretical study using density functional theory (DFT) showed that adsorption is mainly caused by C–H…O, C–H…π, lone-pair…π and π…π interactions. Equilibrium was reached after 120 min, with PAC removing a total of 96.68% of BPA. The best condition was achieved using 0.01 g at pH 9 and 298 K (246.20 mg/g). Good fittings to Dubinin–Raduschkevich (R^2 = 0.985) and to Langmuir (R^2 = 0.925) models were achieved, with a calculated maximum monolayer adsorption capacity (q_{max}) of 367.88 mg/g.

Keywords: Adsorption; DFT calculation; NCI Index; Water treatment

1. Introduction

Water scarcity and increasing problems with water pollution are on the horizon. According to the World Health Organization [1], by 2025 half of the world's population will be living in water-stressed areas. The presence of micropollutants in this remaining water will make water treatment technologies even more important, as many of these substances pose serious health problems when ingested [2].

One emerging micropollutant of great concern is bisphenol A (BPA). BPA is one of the most used synthetic compounds in the world, with an estimated production of nine million tons per year [3,4]. It is extensively used in the production of polycarbonates, epoxy resins, and other polymers [5], and has been receiving growing attention over the last decade since it's an endocrine disruptor linked to several serious health problems, such as breast, prostate, and lung

* Corresponding author.

cancer, as well as negative effects over the reproductive, nervous, and immune systems [6].

One study, investigating the efficiency of different types of water treatment processes in removing endocrine-disrupting chemicals, concluded that the coagulation/flocculation steps, commonly used in conventional water treatment plants, removed only 0%–3% of BPA [7]. Another study, investigating the removal of BPA and analogues in municipal wastewater treatment plants (WWTPs), ranked the following treatment steps in ascending order of efficiency: primary treatment, lagoon process, biological aerated filter, and activated sludge. The authors concluded that sorption and biodegradation were the two main factors involved in BPA removal from wastewater in WWTPs [8].

Adsorption has many advantages, such as simple design, easy operating procedures, and high removal efficiencies [9]. Activated carbon is the most used adsorptive material due to some interesting characteristics, such as its high specific surface area (typically between 500 and 1,500 m²/g) and well-developed porous structure [10]. Several activated carbons have been applied to remove BPA from water, such as granular activated carbon (GAC) made from potato peels, which reached a maximum adsorption capacity (q_{max}) of 454.60 mg/g [11], and two modified commercial GAC, with values of 392.90 and 424.90 mg/g [12]. Powdered activated carbon (PAC) has been applied too, such as the palm-shell waste adsorbent impregnated with magnesium silicate, with a q_{max} equal to 168.4 mg/g [13].

Computational chemistry is an area of chemistry that uses computer science to investigate many properties of molecules, including structure, electron density distributions, vibrational frequencies, among others [14]. Density functional theory (DFT) methods have been used before to investigate BPA with several different purposes, such as synthesizing new less-toxic monomers [14], investigating the main degradation pathway of BPA polycarbonate [15,16], and finding the primary pathway of byproduct formation in a Fenton reactor [17]. The non-covalent interactions (NCI) index is a useful tool to understand NCI, even in large systems such as proteins [18]. It has been applied before in adsorption studies, for example, the acetamiprid adsorption by carbon nanocones [19]. Nevertheless, to the best of our knowledge, there is a lack of studies employing the NCI index to understand the interactions of BPA on the surface of activated carbons. Experimental adsorption studies and theoretical chemistry are not usually combined, although both can benefit from one another, deepening our understanding of how to address water pollution problems. Since activated carbons are widely used in water treatment systems, knowing which interactions are responsible for removing BPA is significant, as it deepens the discussions of adsorption studies, supports the development of new adsorbent materials and gives rise to new treatment conditions in which BPA adsorption is favored.

This study aims to (1) characterize PAC using different techniques; (2) use a computational simulation in order to investigate the behavior of BPA in water and its interaction with a generic carbonaceous surface; and (3) apply kinetically and isotherm models to investigate PAC efficiency in removing BPA from water.

2. Materials and methods

2.1. Materials

Powder activated carbon (Norit® SAE SUPER) was provided by Cabot Brasil Indústria e Comércio Ltda. BPA (≥99% purity) was purchased from Sigma-Aldrich. Physicochemical properties of BPA are given in Table 1. All solutions were prepared using ultrapure water.

2.2. Methods

2.2.1. Characterization of PAC

To determine the point of zero charges (pHPZC), a 0.01 M NaCl solution was prepared. The pH of this solution was corrected to multiple points (2–12), using NaOH and HCl (0.1 or 1.0 M) [25]. After that, Erlenmeyer flasks containing 25 mL of this NaCl solution and 0.05 g of PAC each were placed inside a TE-4200 orbital shaker (Tecnal®), which was kept operating for 24 h at 200 rpm and 298 K. After that, the pH of each solution was measured and used to plot an initial pH vs. final pH graph.

Textural analysis was carried out using an N_2 sorption/desorption analyzer (NOVA 4000e – Quantachrome®). In order to remove water and other contaminants, samples were previously treated in a vacuum system at 353 K for 3 h 30 min. Experiments were performed for 4 h, using gaseous nitrogen as adsorbate and liquid nitrogen as a refrigerant liquid, with 20 adsorption/desorption points. Relative pressures (p/p_0) between 0.04 and 1.00 were used in order to perform this analysis. Then, Brunauer–Emmett–Teller (BET) and *t*-plot methods were employed to calculate the surface area, porevolume, and pore diameter of PAC.

In order to understand the surface morphology of PAC, a scanning electron microscopy (SEM) (VEGA 3 – TESCAN®) was employed.

Table 1
Physicochemical properties of bisphenol A [20–24]
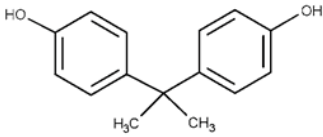
Molecular structure	
IUPAC name	4,4-dihydroxy-2,2-diphenylpropane
Molecular formula	$C_{15}H_{16}O_2$
Molecular weight	228.29 g/mol
pKa	9.6–10.2
LogK_{ow}	3.4
Solubility in water	300 mg/L
Maximum adsorption wavelength	276 nm
Uses	Production of polycarbonate and epoxy resins
Appearance	White powder

Functional groups were characterized by Fourier transform infrared spectroscopy (FTIR) (1725X – Perkin Elmer®) using KBr discs. Before this analysis, PAC was dried at 110°C for 1 h. Crystalline structure was analyzed by X-ray diffraction (XRD) (7000 – Shimadzu®) with Cu-Kα radiation.

2.2.2. Theoretical studies

To assess the interactions between BPA and PAC, as well as their structural features in solution on a microscopic level, electronic structure calculations were performed. Given that there is no information on how the Norit® SAE SUPER activated carbon is prepared, or on what is used as the raw material, the carbonaceous structure employed was built based on a literature review [26,27] and FTIR and DRX results found in this study. The molecular structure of PAC was modeled based mainly on a study [26], in which infrared spectroscopy showed that graphene oxide exhibited very similar characteristics to PAC. Thus, the molecular structure for PAC has dimensions L_1 = 1.68 nm and L_2 = 1.57 nm, with an area of 0.26 nm³, while the BPA molecule has dimensions of L_1 = 0.99 nm, L_2 = 0.79 nm, and L_3 = 0.44 nm.

The BPA + PAC molecules were placed in the center of a cubic cell and solvated with 64 water molecules. This number of water molecules is known to be a minimum amount to avoid the finite size effect in simulations in an aqueous medium [28]. A structure optimization was performed employing the DFT formalism, using the Perdew, Burke, and Ernzerhof (PBE) [29] generalized gradient approximation (GGA) for the exchange-correlation functional. Ultrasoft pseudopotentials available from Pslibrary 1.0.0 [30] were used to represent effective nuclei. A kinetic energy cutoff of 100 RY was found to be suitable, providing an energy convergence of better than 2 meV per atom. Grimme's dispersion correction (D2) [31] was included for all atoms. These calculations were performed using the plane wave code Quantum ESPRESSO [32] version 6.0.

In order to identify and characterize the interactions between BPA and PAC (hydrogen bonds, van der Waals forces, repulsive, and attractive steric interactions), the NCI [33] approach was applied for stable geometry. Since it's based on electron density and reduced gradients, this approach is capable of revealing very weak interactions, of low electron density, using only molecular geometry information. This method provides a representation of the intra- and inter-molecular interactions through surfaces generated by the NCIPLOT [18] software.

2.2.3. Adsorption studies

Removal efficiency and equilibrium adsorption quantity were calculated using Eqs. (1) and (2), respectively [34], in which C_0 and C_e are the initial and the equilibrium BPA concentrations (mg/L), respectively; V is the solution volume (L); and m is the mass of adsorbent (g).

$$R(\%) = \frac{(C_0 - C_e)}{C_0} \cdot 100 \tag{1}$$

$$q_e = \frac{(C_0 - C_e) \cdot V}{m} \tag{2}$$

2.2.4. Kinetics

Kinetic experiments were conducted using 0.01 g of PAC and 25 mL of a 100 mg/L BPA solution with pH adjusted to 7. This pH condition was chosen based on pKa and pH$_{PZC}$ of BPA and PAC, respectively. Adsorbent and solution were placed inside a 125 mL Erlenmeyer flask, which was positioned inside a TE-4200 orbital incubator shaker (Tecnal®) that was kept operating at 200 rpm and 25°C ± 2°C. At different intervals (5–300 min), 10 mL samples were collected and centrifuged at 4,000 rpm for 5 min. The supernatant was analyzed at 276 nm using a UV-vis spectrophotometer [35]. In order to quantify the amount of BPA in solution after treatment, analytical curves were prepared with concentrations ranging from 0.5 to 60 mg/L.

Pseudo-first-order (PFO), pseudo-second-order (PSO), as well as intraparticle diffusion, were employed to evaluate the adsorption kinetic behavior (Table 2).

2.2.5. Influence of pH and mass

The second test was performed to analyze the influence of adsorbent mass (0.01, 0.02, 0.03, and 0.04 g) and solution pH (2, 4, 7, 9, and 12) over the adsorption capacity of PAC. In order to carry out this test, 25 mL of a 100 mg/L BPA solution was placed inside a 125 mL Erlenmeyer flask. After 3 h in the incubator shaker operating at 200 rpm, samples (10 mL) were collected and centrifuged as reported before. Experiments were performed in triplicate.

2.2.6. Isotherms

In order to investigate BPA removal by PAC using isotherm models, the best condition of mass, and pH was employed, together with 25 mL of varied BPA concentrations (50, 75, 100, 125, 150, and 175 mg/L). Samples were

Table 2
Pseudo-first-order, pseudo-second-order, and intraparticle diffusion kinetic models [34]

Model	Equation	Equation number
Pseudo-first-order	$\log(q_e - q_t) = \log(q_e) - \dfrac{k_1 \cdot t}{2.303}$	Eq. (3)
Pseudo-second-order	$\dfrac{t}{q} = \dfrac{1}{k_2 \cdot q_e^2} + \dfrac{t}{q_e}$	Eq. (4)
Intraparticle diffusion	$q_t = k_p \cdot \sqrt{t} + C$	Eq. (5)

Note: (q_e) is the mass of BPA adsorbed at equilibrium (mg/g); (q_t) is the mass of BPA adsorbed at time t (mg/g); (k_1) is the pseudo-first-order constant (min⁻¹); (k_2) is the pseudo-second-order constant (g/mg min); and (k_p) is the intraparticle diffusion constant (mg/g min¹/²).

placed inside Erlenmeyer flasks, shaken for 3 h, centrifuged, and analyzed as described before. Langmuir, Freundlich, Dubinin–Radushkevich, and Redlich–Peterson models were applied to evaluate the data obtained (Table 3).

3. Results and discussion

3.1. Characterization of PAC

To determine the superficial charge density of PAC in a certain solution pH, the pH_{PCZ} analysis was performed. This is an important analysis for adsorbents, as it indicates whether the material is positively charged ($pH_{solution} < pH_{PCZ}$), facilitating the removal of anions, or negatively charged ($pH_{solution} > pH_{PCZ}$), attracting cations in solution [36]. The point of zero charges (pH_{PZC}) was equal to 6.29. BPA is ionized to form bisphenolate anions at pH between 9 and 10 [37], and at this same pH, PAC is negatively charged. It was expected, consequently, that pH conditions greater than 9 would result in lower removal efficiencies.

Textural analysis of PAC was performed in order to investigate its specific and external areas, as well as its porous structure. The sorption/desorption of N_2 was employed, and results were evaluated using BET and *t*-plot methods. Results can be seen in Table 4.

PAC has a high specific area (851.0 m²/g), and an external area of 156.6 m²/g. The difference between these two results (694.4 m²/g) shows that PAC's high specific area is mainly due to its internal structure, the consequence of a well-developed porosity. According to Dubinin's classification, PAC is in the mesoporous range (average pore radius: 1.36 nm). This material also presented a type IV(a) isotherm, which confirms its mesoporous nature [38]. Mesopores are essential [39], especially for larger molecules, as an increase in pore size facilitates adsorption kinetics and regeneration of the adsorbent [40]. The larger distance in BPA molecule (0.94 nm) is related to the –OH groups located in both

aromatic rings. BPA's height corresponds to 0.53 nm, the benzene ring's width is 0.43 nm and the superficial area is equal to 4.32 nm² [41]. The average pore diameter in PAC is 2.72 nm, indicating that BPA had access to PAC's internal porous structure, which increased PAC's efficiency in removing this contaminant.

SEM image can be seen in Fig. 1. SEM showed that PAC particles are compacted and unevenly distributed in the samples. The particles have small cavities and rough areas with pores on their surface, confirming the results of BET for this material, which have already indicated a highly porous material.

PAC was also characterized by FTIR and XRD analysis (Fig. S1). FTIR spectrum (Fig. S1a) shows an intense peak next to 3,500 cm⁻¹, which corresponds to stretching of –OH groups from water or oxygenated functional groups such as alcohol and carboxylic acids. PAC also showed a peak near 1,635 cm⁻¹, which can be attributed to the stretching of C=C bonds (1,900–1,500 cm⁻¹). Furthermore, signals that appear

Table 4
Textural analysis of PAC obtained with N_2 sorption/desorption technique analyzed by BET and *t*-plot equations

Specific area (m²/g)	851.0
External area (m²/g)	156.6
Micropore area (m²/g)	694.4
Micropore volume (cm³/g)	0.357
Total pore volume (cm³/g)	0.579
Average pore radius (nm)	1.36

Table 3
Langmuir, Freundlich, Dubinin-Radushkevich and Redlich-Peterson isotherm models [34]

Model	Equation	Equation number
Langmuir	$q_e = \dfrac{q_{max} b C_e}{1 + b C_e}$	Eq. (6)
Freundlich	$q_e = K_F C_e^n$	Eq. (7)
Redlich–Peterson	$q_e = \dfrac{K_{RP} C_e}{1 + \alpha_{RP} C_e^g}$	Eq. (8)
Dubinin–Radushkevich	$q_e = q_{DR} \exp\left(-K_{DR} \varepsilon^2\right)$	Eq. (9)

Note: (q_{max}) is the maximum monolayer adsorption capacity (mg/g); (*b*) is the Langmuir constant (L/mg); (K_F) is the Freundlich constant (mg/g)/(mg/L)ⁿ; (*n*) is the heterogeneity factor (dimensionless); (K_{RP}) and (α_{RP}) are the Redlich–Peterson constants (L/g) and (mg/L)⁻ᵍ, respectively; (*g*) is the exponent that must lie between 0 and 1 (dimensionless); (q_{DR}) is the adsorption capacity (mg/g); (K_{DR}) is the constant related to the sorption energy (mol²/kJ²); (ε) is the Polanyi potential.
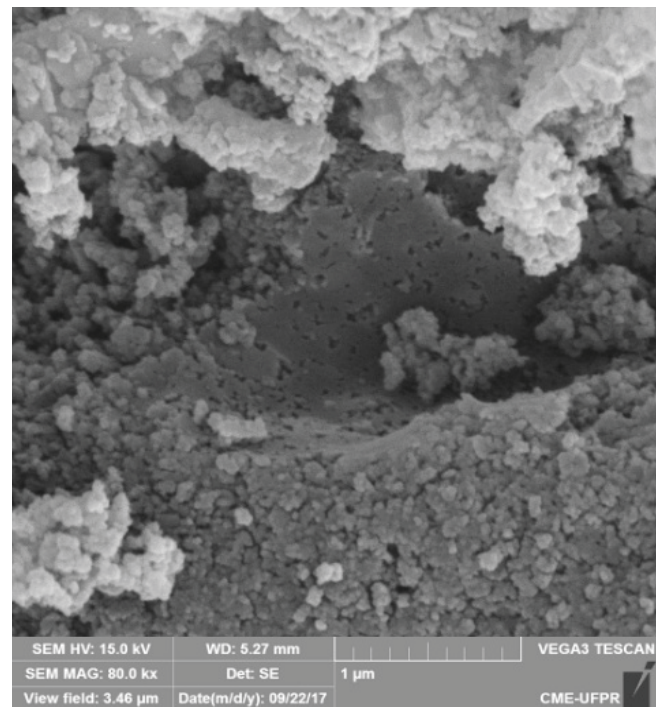

Fig. 1. Scanning electron microscopy (SEM) image of PAC (80,000×).

between 1,500 and 650 cm^{-1} indicate the presence of C–O bonds [42]. FTIR indicates that this adsorbent possesses, mainly, –OH groups on its surface. This is an interesting feature, as these –OH groups can be potential interaction points between PAC and contaminants.

In XRD results (Fig. S1b), PAC showed two intense peaks, one near 26 and another near 44, both related to Bragg's reflection of the (002) and (100) planes, respectively. These peaks correspond to the mineralogical phase of graphite [43,44], which is associated with the processes of graphitization and the formation of a nanocrystalline structure, which was expected to be present. Also, peak width indicates that PAC has an amorphous structure [45]. The basic surface of carbon materials is made of carbon atoms arranged in fused aromatic rings, mainly exhibiting sp^2-hybridization. Van der Waals interactions are responsible for maintaining graphene layers stacked on top of each other [27]. This stacking can either form a disordered structure (also called a turbostratic structure), or an ordered structure (graphitic). The turbostratic structure is found in activated carbons [27], and is interesting because of its high porosity and surface area when compared to a graphitic structure [46].

3.2. Theoretical studies

The FTIR spectrum of PAC (Fig. S1a) provided evidence that this material has some oxygenated functional groups on its surface, such as alcohol and carboxylic acids, as well as peaks associated with C=C bonds. This result was used, together with a literature review [26,27], to propose a generic carbonaceous structure (Fig. 2a) to further investigate BPA and PAC interactions using computational simulation (Fig. 2b).

Fig. 2b shows the structure obtained after a geometry optimization, where the BPA molecule interacts with the surface of PAC mainly by dispersion interactions, while the water molecules prefer the hydrogen bonding sites of the hydroxyl, carbonyl, and pyran groups located on the edges and face of the activated carbon structure.

The 3D isosurfaces, showing the nature of the inter- and intra-molecular interactions, are depicted in Fig. 3. They allow visualization of NCI as large regions of real space according to the density in the respective interatomic interaction.

Fig. 3 shows the density surface between the overlapping moieties of the phenyl ring and activated carbon surface, where the π-stacking is expected. It was possible to identify C–H…O, C–H…π, lone-pair…π and π…π interactions between BPA and activated carbon, which are represented in green. Also, red regions of nonbonded overlap located at the center of each ring are shown. More intense attractive interactions, such as hydrogen bonds or electrostatic interactions, are represented in a blue-green scale.

The NCI analysis also provided a graph (Fig. 4) of the reduced density gradient (RDG) as a function of the density (ρ). The sign(λ_2)ρ describes attractive (large negative values) interactions such as dipole-dipole or hydrogen bonding, and nonbonding interactions (large positive values). Values near zero indicate very weak, van der Waals interactions.

Therefore, the troughs in range of −0.01 and +0.01 correspond to the weak C–H…π, lone-pair…π and π…π and dispersion H...H interactions, represented in green in the RDG isosurface (Fig. 4). These interactions are responsible for stabilizing the BPA molecule on the activated carbon surface. The interactions at sign(λ_2)ρ 0.025 a.u. have one trough with a negative value and one trough with a positive value, corresponding to an attractive steric force (blue–green color scale of the RDG isosurface) and a repulsive steric force (green–red color scale of the RDG isosurface), respectively. This is due to ring formation, which results in C–H…O and H…H intramolecular interactions in the activated carbon. The positive troughs from +0.045 to +0.055 a.u. sign(λ_2)ρ values correspond to the non-bonded overlap located at the center of each benzene and furyl ring (red color), respectively. NCI analysis was successfully applied to characterize and quantify similar interactions in some substituted furans [47].
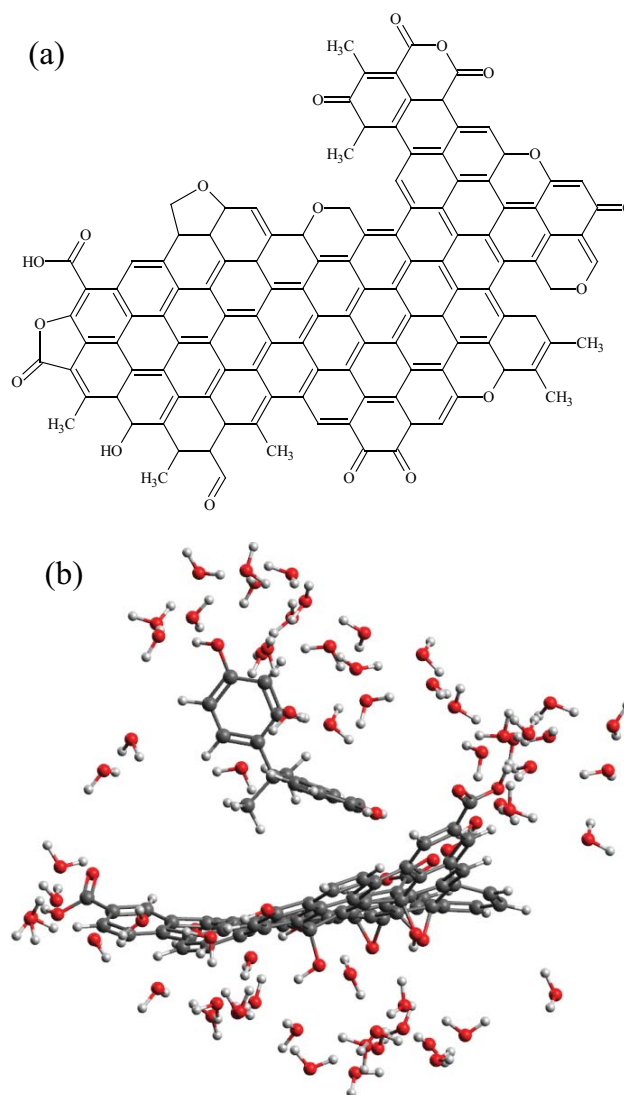

Fig. 2. Structure of: (a) generic activated carbon and (b) BPA interacting with PAC in solution.
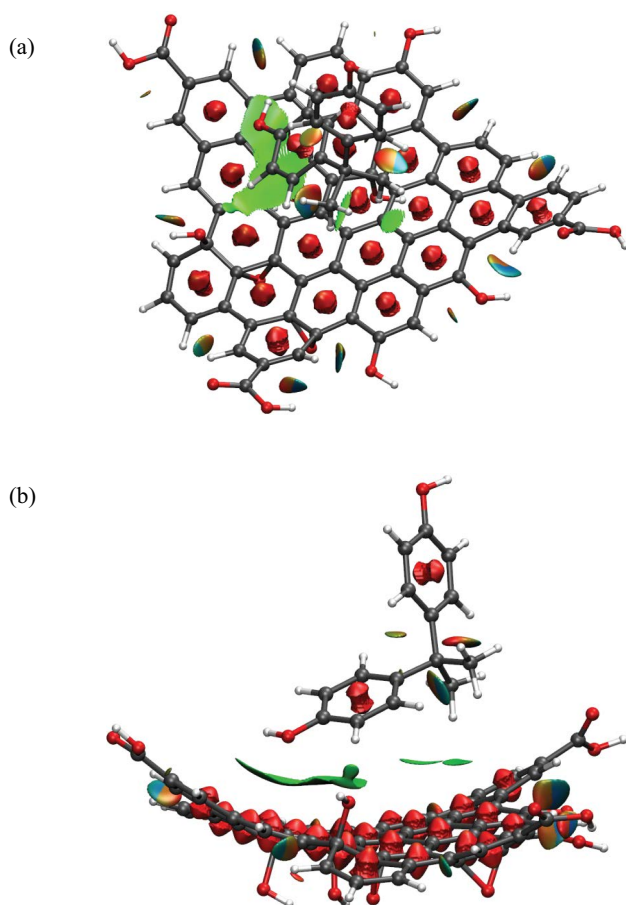
Fig. 3. NCI isosurfaces for the BPA + activated carbon complex from top (a) and side view (b). RDG isosurface value: 0.3 a.u., and a blue–green–red color scale from $-0.04 <$ sign $(\lambda_2)\rho < 0.04$ a.u. The water molecules were stripped for better visualization of the BPA-activated carbon interactions (for interpretation of the references to color in this figure legend, the reader is referred to the web version of this article).
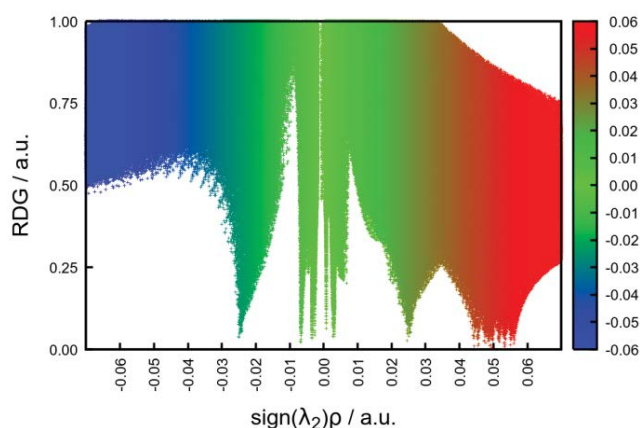

Fig. 4. Plots of the reduced density gradient (RDG) vs. sign $(\lambda_2)\rho$ of BPA + activated carbon.

3.3. Adsorption studies

3.3.1. Kinetic study

Adsorption studies were initiated with kinetic experiments (Fig. 5). Kinetic parameters are very important to be established since adsorbents with high adsorption rates are considered ideal for water treatment systems [48]. PAC was able to remove 90.88% of BPA in 5 min and a total of 96.68% after 120 min, the time when it reached equilibrium.

In one study that investigated BPA removal by activated carbon made from palm oil extraction residue, 48 h were necessary for the system to reach equilibrium, achieving 96.10% of BPA reduction [49]. The authors needed two days to reach a result similar to that obtained in 2 h with PAC. In another study, which investigated BPA adsorption using two commercially available granular activated carbons (vegetal and bituminous), 8 and 4 h were needed, respectively, for equilibrium to be reached [50]. These results indicate that PAC used in this study is an excellent option to remove BPA from water.

Kinetic data were adjusted to PFO, PSO, and intraparticle diffusion models. The best adjustment was achieved with the PSO equation (Fig. 5b). Data was not properly fitted to the PFO model (Fig. S2). Kinetic parameters obtained with these models can be seen in Table 5.

A calculated q_e equal to 229.88 mg/g and a constant (k_2) of 0.77×10^{-4} g/mg min were obtained from the PSO equation. The calculated q_e is in good agreement with the experimental q_e (229.20 mg/g), which indicates, together with R^2 (0.999), that PSO is the best model to describe this kinetic experiment. PSO model suggests chemical adsorption [51]. The result found for the parameter q_e (mass of BPA adsorbed at equilibrium, in mg/g), is superior to many others found in literature, such as the ones obtained using activated carbon made from palm oil extraction residue (19.28 mg/g) [49], modified zeolite (114.90 mg/g) [52], and graphene (182.00 mg/g) [53]. The activated carbon made from palm oil residue also had an inferior k_2 value $(0.03 \times 10^{-4}$ g/mg min), which indicates that commercial PAC used in this study is faster in removing the same compound from water.

PAC data was not well-fitted to PFO model ($R^2 = 0.712$). This poor fitting can be noted from the difference between the calculated q_e (7.55 mg/g), and the one obtained experimentally (229.20 mg/g). For k_1, the PFO constant, a value equal to 0.01 min^{-1} was achieved. This is similar to those obtained when removing BPA using one granular activated carbon and one made from black-tea waste, equal to 0.02 and 0.01 min^{-1}, respectively [54].

The data were also fitted to the intraparticle diffusion model. If a linear relationship between q_t and $t^{1/2}$ is obtained with kinetic data, intraparticle diffusion can be considered the main mechanism of sorption [55]. If the linear relationship also passes through the origin, intraparticle diffusion is the only limiting step of adsorption. Data also indicates that adsorption is controlled by more than one mechanism when a multi-linear relationship is observed [56]. As it can be seen in Fig. 6, q_t vs. $t^{1/2}$ forms a multi-linear relationship with at least two distinct regions (different angular coefficients), indicating that BPA removal by PAC is controlled by more than one mechanism: an initial step of diffusion in the
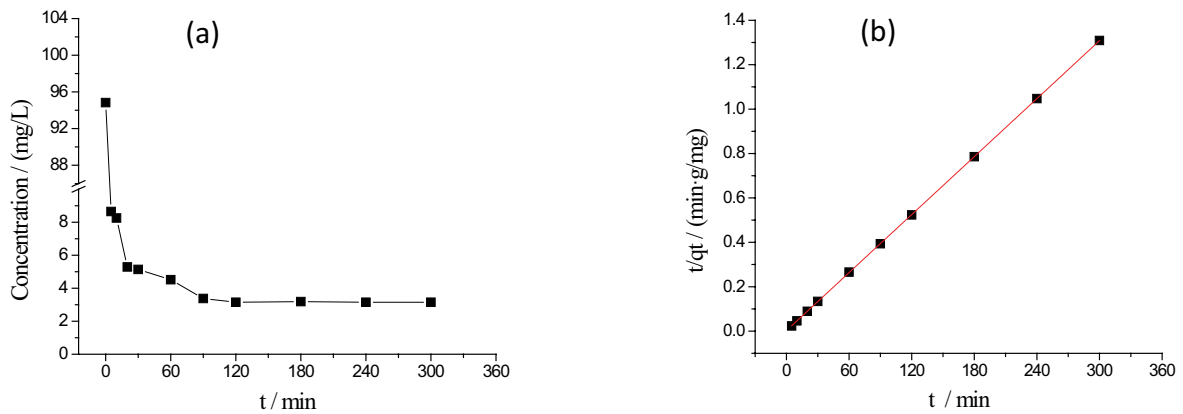
Fig. 5. Kinetic study of bisphenol A removal in PAC evaluated by (a) *t* x concentration and (b) pseudo-second-order model (0.01 g of adsorbent; 25 mL of 100 mg/L BPA solution; pH 7; 200 rpm; 25°C ± 2°C).

Table 5
Kinetic parameters of bisphenol A removal in PAC obtained with pseudo-first-order (PFO), pseudo-second-order (PSO) and intraparticle diffusion models

Model	Equation	R^2	k_1	$q_{e,cal}$	
PFO	$\log(q_e - q_t) = 0.878 - 0.0045 \cdot t$	0.712	0.01	7.55	
			k_2	$q_{e,cal}$	$q_{e,exp}$
PSO	$t/q_t = 0.00247 + 0.00435 \cdot t$	0.999	0.77×10^{-4}	229.88	229.20
			k_p	C	
Intraparticle diffusion	$q_t = 211.58 + 1.87\ t^{1/2}$	0.926	1.87	211.58	

Note: (q_e) is the mass of BPA adsorbed at equilibrium (mg/g); (k_1) is the pseudo-first-order rate constant (min^{-1}); (k_2) is the pseudo-second-order rate constant (g/mg min); (k_p) is the intraparticle diffusion constant (mg/g min$^{1/2}$); (C) is the intraparticle diffusion constant associated to the boundary layer width (mg/g).
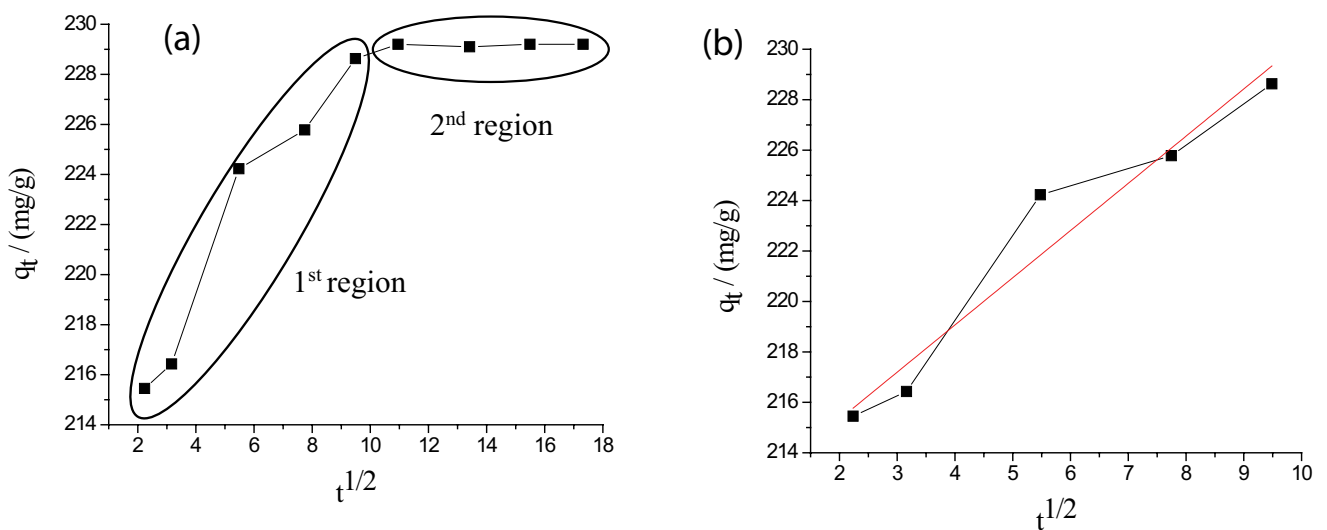

Fig. 6. Bisphenol A adsorption in PAC evaluated by intraparticle diffusion model, in: (a) all data interval and (b) first region.

adsorbent surface and the second step of equilibrium condition. Since the lines don't pass through the origin, it can be concluded that intraparticle diffusion is not the only limiting step [56].

Linear adjustment applied to the first portion of Fig. 6a can be seen in Fig. 6b. Intraparticle diffusion constant, C, indicates the amount of contaminant adsorbed up to the limit layer [34], and was equal to 211.58 mg/g, close to what was obtained for q_e (229.88 mg/g).

3.3.2. Influence of pH and mass

Adsorption was evaluated using different masses of PAC and solution pH, in order to investigate the effect of both variables over the adsorptive capacity (q_e). Results can be seen in Fig. 7.

A general trend of reduction of q_e with increasing masses of PAC was observed. This trend is reported by other researchers [57,58], and explained by a decrease in surface area and adsorption sites available to remove the contaminant, caused by the adsorbent aggregation in higher doses [59]. The highest $q_{e,exp}$ with PAC was achieved with 0.01 g at pH 9 (246.20 mg/g). Nevertheless, variations in results using different pH with the same mass of adsorbent were very small. Using 0.01 g of PAC, pH 12 was the condition in which PAC removed less BPA (232.39 mg/g).

In a study that investigated removing BPA with two granular activated carbons (coconut shell and bituminous) at different pH levels (3, 5, 7, 9, and 11), a similar result was achieved. Using the bituminous carbon, the highest q_e was obtained at pH 9 (239.10 mg/g) and the lowest q_e at pH 11 (196.10 mg/g) [60]. In another investigation, in which two commercial activated carbons were modified by acidic and thermal treatment, the worst adsorption capacity was also observed at pH 11 [12]. This tendency is explained by the pK_a value of BPA, which lies between 9.6 and 10.2 and causes it to ionize and form bisphenolate anions at pH between 9 and 10 [60]. The reduction of q_e at high pH values (>10) is probably

caused by repulsion between bisphenolate anions and the negative charge of oxygenated functional groups on the carbon surface [60]. This reduction of q_e at higher solution pH is in good agreement with the pH_{PZC} of PAC (6.29), which also points to the existence of a negatively charged surface in this adsorbent ($pH_{solution} > pH_{PCZ}$).

Based on this investigation, the mass and pH conditions chosen to be applied in the isotherm studies were 0.01 g and pH 9, as this combination provided the highest value of adsorption capacity.

3.3.3. Isotherm studies

The adsorption isotherm of BPA in PAC adjusted to non-linear Dubinin–Radushkevich, Redlich–Peterson, Langmuir, and Freundlich models can be seen in Fig. 8.

Isotherms like the ones in Fig. 8, characterized by an ascending convex curvature, are classified as favorable or highly favorable [61]. This behavior is expected, as increasing concentrations provide a driving force to overcome the mass transfer resistance between adsorbent and adsorbate [62]. Parameters obtained with Dubinin–Radushkevich, Redlich–Peterson, Langmuir, and Freundlich isotherm models can be seen in Table 6. The non-linear forms of the equations were applied, since the transformation of data into linear fittings can introduce unnecessary errors, altering the weight placed on each experiment point [34].

Data was best described by the DR equation ($R^2 = 0.985$), followed by RP ($R^2 = 0.942$), Langmuir ($R^2 = 0.925$), and Freundlich ($R^2 = 0.788$) models.

DR was developed in order to encompass the effects of the adsorbent porous structure. An adsorption capacity of 318.43 mg/g and a constant K_{DR} equal to 7.92×10^{-7} mol²/kJ² were obtained.

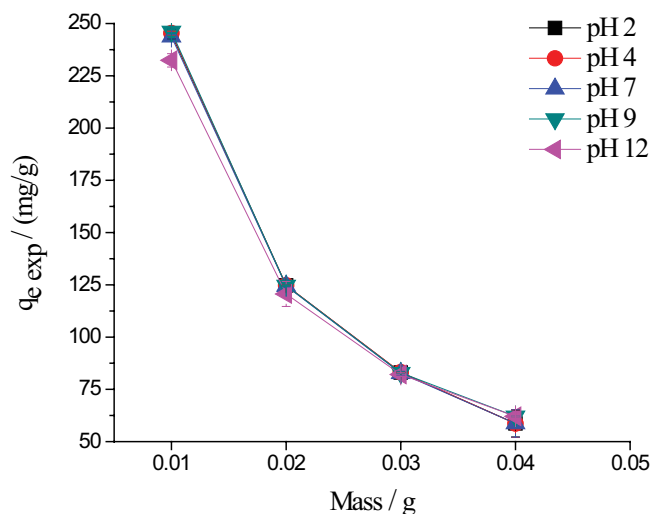Although a good R^2 was obtained when using the RP model ($R^2 = 0.942$), g (1.24) indicates that the data is not

Fig. 7. Adsorption capacity values ($q_{e,exp}$) of BPA removal by PAC (0.01–0.04 g of adsorbent; 25 mL of 100 mg/L BPA solution; 200 rpm; 25°C ± 2°C; 3 h).
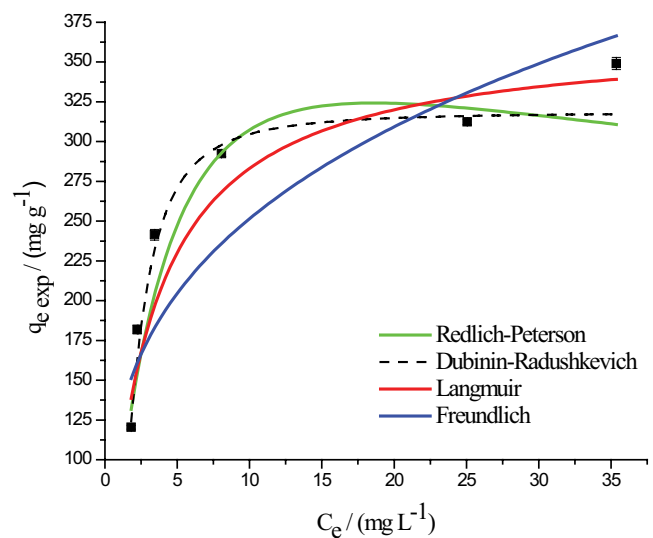

Fig. 8. Adsorption isotherm of BPA in PAC, adjusted to Dubinin–Radushkevich, Redlich–Peterson, Langmuir, and Freundlich models (0.01 g of PAC; 25 mL of 50–175 mg/L BPA solution; pH 9; 200 rpm; 25°C ± 2°C; 3 h).

Table 6
Dubinin–Radushkevich, Redlich–Peterson, Langmuir, and Freundlich parameters of BPA removal by PAC

Model	Non-linear equation	R^2	Parameter	Result
DR	$q_{e,exp} = 318.43 \cdot e^{(-7.92 \times 10^{-7} \, \varepsilon^2)}$	0.985	q_{DR} (mg/g)	318.43
			K_{DR} (mol²/kJ²)	7.92×10^{-7}
RP	$q_{e,exp} = (89.40 \cdot C_e)/(1 + 0.11 \cdot C_e^{1.24})$	0.942	K_{RP} (L/mg)	89.40
			α_{RP} (mg/L)$^{-g}$	0.11
			g	1.24
Langmuir	$q_{e,exp} = (367.88 \cdot 0.334 \cdot C_e)/(1 + 0.334 \cdot C_e)$	0.925	q_{max} (mg/g)	367.88
			b (L/mg)	0.334
Freundlich	$q_{e,exp} = 126.62 \cdot C_e^{0.298}$	0.788	n	0.298
			K_F ((mg/g)/(mg/L)^n)	126.62

Note: (q_{max}) is the maximum monolayer adsorption capacity (mg/g); (b) is the Langmuir constant (L/mg); (K_F) is the Freundlich constant (mg/g)/(mg/L)^n; (n) is the heterogeneity factor (dimensionless); (K_{RP}) and (α_{RP}) are the Redlich–Peterson constants (L/g) and (mg/L)$^{-g}$, respectively; (g) is the exponent that must lie between 0 and 1 (dimensionless); (q_{DR}) is the adsorption capacity (mg/g); (K_{DR}) is the constant related to the sorption energy (mol²/kJ²); (ε) is the Polanyi potential.

properly explained by this model, as this parameter is not inside the range of 0–1 [34].

For a good adsorbent, a high maximum monolayer adsorption capacity (q_{max}) and a steep slope in the first portion of its isotherm (high value for the Langmuir constant – b) are expected, being b a parameter related to the affinity between adsorbent and adsorbate [34]. Although the data showed a less proper fitting to the Langmuir model when compared to the DR model, the parameter q_{max} is commonly used in adsorption studies to compare different adsorbents as to their capacity to remove pollutants from water. Therefore, Langmuir parameters are also used in this study. Langmuir is based on the following principles: (1) molecules are adsorbed in specific sites in the adsorbent surface, with all sites having the same adsorption energy; (2) adsorption is reversible; (3) when the contaminant molecule occupies one site, this site becomes unavailable to other adsorptions to occur; (4) there is no interaction between adsorbed molecules; (5) a monolayer formation occurs; (6) adsorbent surface is considered homogeneous; and (7) intensity of intermolecular attraction forces decrease rapidly with increasing distance [34,63]. A q_{max} equal to 367.88 mg/g and b equal to 0.334 L/mg were obtained from the Langmuir equation. In another study that investigated the removal of BPA by powdered activated carbon, a q_{max} equal to 354.71 mg/g and b equal to 0.230 L/mg were obtained [64]. This value of q_{max} is very similar to that obtained in the present study. However, b value is inferior, indicating that PAC used here presents greater affinity to BPA.

A comparison of literature data of BPA adsorption obtained with the use of varied materials can be seen in Table 7.

The maximum monolayer adsorption capacity (q_{max}) of PAC is inferior to those of other materials, such as activated carbon made from potato peels (454.60 mg/g) However, it is superior to many others, for example, the modified zeolite (114.90 mg/g) used by Dong et al. [52]. This parameter alone, however, does not fully indicate the best adsorbent to be used in real treatment systems, since the material can remove a great amount of BPA, but demands a long time to

Table 7
Values of maximum monolayer adsorption capacity (q_{max}) for BPA removal in different adsorbents

Adsorbent	q_{max} (mg/g)	Reference
Potato peels GAC	454.60	[11]
Modified commercial GAC	424.90	[12]
Modified commercial GAC	392.90	[12]
PAC Norit® SAE-super	367.88	Present study
Commercial PAC	354.71	[64]
Graphene	182.00	[53]
Modified zeolite	114.90	[52]
Graphene	94.06	[65]
Graphene oxide	49.26	[66]
Graphene oxide	17.27	[65]
Commercial GAC	16.26	[54]
Black tea leaves GAC	18.35	[54]
Hydrogel of βCD and HPMC	14.60	[67]
Graphene	2.00	[68]

Legend: (βCD) is the β-ciclodextrin; (HPMC) is the hidroxipropil metilcelulose.

reach equilibrium. GAC made from potato peels reached the highest q_{max}, as can be seen in Table 6. Nevertheless, 24 h were necessary to perform isothermal experiments, while 2 h were enough for PAC to reach equilibrium. This means that PAC should be considered a very interesting material to enhance the performance of water treatment systems in removing BPA and possibly other organic contaminants from water.

4. Conclusion

The main conclusions are: (1) the C–H…O, C–H…π, lone-pair…π and π…π interactions between BPA and activated carbon were identified through DFT, being them responsible for BPA adsorption; (2) PSO was the best model to describe kinetic data ($R^2 = 0.999$) and equilibrium was reached after 120 min, with a total of 96.68% of BPA

removal; (3) PAC was not greatly affected by pH variations (2–12), maintaining a similar efficiency in varied conditions, which is interesting for real water treatment systems; (4) data was better described by Dubinin–Radushkevich isotherm model (R^2 = 0.985), with a q_{DR} of 318.43 mg/g and a constant K_{DR} equal to 7.92×10^{-7} mol^2/kJ^2; and (5) Langmuir model was also applied, providing a calculated q_{max} equal to 367.88 mg/g, which represents a higher efficiency in comparison to other adsorbents described in the literature.

Acknowledgments

References

[1] Available at: https://www.who.int/news-room/fact-sheets/detail/drinking-water (accessed March 12, 2021).

[2] H.B. Quesada, A.T.A. Baptista, L.F. Cusioli, D. Seibert, C.O. Bezerra, R. Bergamasco, Surface water pollution by pharmaceuticals and an alternative of removal by low-cost adsorbents: a review, Chemosphere, 222 (2019) 766–780.

[3] N. Jalal, A.R. Surendranath, J.L. Pathak, S. Yu, C.Y. Chung, Bisphenol A (BPA) the mighty and the mutagenic, Toxicol. Rep., 5 (2018) 76–84.

[4] R. Gerona, F.S. Vom Saal, P.A. Hunt, BPA: have flawed analytical techniques compromised risk assessments, Lancet Diabetes Endocrinol., 8 (2019) 11–13.

[5] S. Almeida, A. Raposo, M.A. González, C. Carrascosa, Bisphenol A: food exposure and impact on human health, Compr. Rev. Food Sci. Food Saf., 17 (2018) 1503–1517.

[6] Y. Ma, H. Liu, J. Wu, L. Yuan, Y. Wang, X. Du, R. Wang, P.W. Marwa, P. Petlulu, X. Chen, H. Zhang, The adverse health effects of bisphenol A and related toxicity mechanisms, Environ. Res., 176 (2019) 1–17.

[7] K.J. Choi, S.G. Kim, C.W. Kim, J.K. Park, Removal efficiencies of endocrine disrupting chemicals by coagulation/flocculation, ozonation, powdered/granular activated carbon adsorption, and chlorination, Korean J. Chem. Eng., 23 (2006) 399–408.

[8] H. Wang, Z.H. Liu, J. Zhang, R.P. Huang, H. Yin, Z. Dang, P.X. Wu, Y. Liu, Insights into the removal mechanisms of bisphenol A and its analogues in municipal wastewater treatment plants, Sci. Total Environ., 692 (2019) 107–116.

[9] M.A. Al-Ghouti, D. Da'ana, M.A. Dieyeh, M. Khraisheh, Adsorptive removal of mercury from water by adsorbents derived from date pits, Sci. Rep., 9 (2019) 1–15.

[10] J. Saleem, U.B. Shahid, M. Hijab, H. Mackey, G. McKay, Production and applications of activated carbons as adsorbents from olive stones, Biomass Convers. Biorefin., 9 (2019) 775–802.

[11] A.C. Arampatzidou, E.A. Deliyanni, Comparison of activation media and pyrolysis temperature for activated carbons development by pyrolysis of potato peels for effective adsorption of endocrine disruptor bisphenol-A, J. Colloid Interface Sci., 466 (2016) 101–112.

[12] G. Liu, J. Ma, X. Li, Q. Qin, Adsorption of bisphenol A from aqueous solution onto activated carbons with different modification treatments, J. Hazard. Mater., 164 (2009) 1275–1280.

[13] C.E. Choong, S. Ibrahim, Y. Yoon, M. Jang, Removal of lead and bisphenol A using magnesium silicate impregnated palm-shell waste powdered activated carbon: comparative studies on single and binary pollutant adsorption, Ecotoxicol. Environ. Saf., 148 (2018) 142–151.

[14] F. Tirgir, M.R. Sabzalian, G. Moghadam, Fabrication and DFT structure calculations of novel biodegradable diphenolic monomer containing D-4-hydroxyphenylglycine moiety as biologically active substituent: compression with toxic industrial bisphenol-A, Des. Monomers Polym., 18 (2015) 401–412.

[15] J. Huang, C. He, X. Li, G. Pan, H. Tong, Theoretical studies on thermal degradation reaction mechanism of model compound of bisphenol A polycarbonate, Waste Manage., 71 (2018) 181–191.

[16] A. Motta, F.P. La Mantia, L. Ascione, M.C. Mistretta, Theoretical study on the decomposition mechanism of bisphenol A polycarbonate induced by the combined effect of humidity and UV irradiation, J. Mol. Graphics Modell., 99 (2020) 107622 (1–4), doi: 10.1016/j.jmgm.2020.107622.

[17] F. Dai, X. Fan, G.R. Stratton, C.L. Bellona, T.M. Holsen, B.S. Crimmins, X. Xia, S.M. Thagard, Experimental and density functional theoretical study of the effects of Fenton's reaction on the degradation of Bisphenol A in a high voltage plasma reactor, J. Hazard. Mater., 308 (2016) 419–429.

[18] J. Contreras-Garcia, E.R. Johnson, S. Keinan, R. Chaudret, J.P. Piquemal, D.N. Beratan, W. Yang, NCIPLOT: a program for plotting noncovalent interaction regions, J. Chem. Theory Comput., 7 (2011) 625–632.

[19] E. García-Hernández, L. Palomino-Asencio, R. Catarino-Centeno, J. Nochebuena, D. Cortés-Arriagada, E. Chigo-Anota, *In silico* study of the adsorption of acetamiprid on functionalized carbon nanocones, Physica E, 128 (2020) 114516 (1–8), doi: 10.1016/j.physe.2020.114516.

[20] W.T. Tsai, H.C. Hsu, T.Y. Su, K.Y. Lin, C.M. Lin, Adsorption characteristics of bisphenol-A in aqueous solutions onto hydrophobic zeolite, J. Colloid Interface Sci., 299 (2006) 513–519.

[21] F.M. Elshaer, A.A.S. Walid, A.B. Sayed, Histopathological changes in the kidney of mosquito fish, *Gambusia affinis* and guppy fish, *Poecilia reticulata* exposed to Bisphenol A, Egypt J. Aquat. Biol. Fish, 17 (2013) 83–93.

[22] A. Shareef, M.J. Angove, J.D. Wells, B.B. Johnson, Aqueous solubilities of estrone, 17β-estradiol, 17α-ethynylestradiol, and bisphenol A, J. Chem. Eng. Data, 51 (2006) 879–881.

[23] L. Patrolecco, S. Capri, S. Angelis, S. Polesello, S. Valsecchi, Determination of endocrine disrupting chemicals in environmental solid matrices by extraction with a non-ionic surfactant (Tween 80), J. Chromatogr. A, 1022 (2004) 1–7.

[24] W. Wang, C. Jiang, L. Zhu, N. Liang, X. Liu, J. Jia, C. Zhang, S. Zhai, B. Zhang, Adsorption of bisphenol A to a carbon nanotube reduced its endocrine disrupting effect in mice male offspring, Int. J. Mol. Sci., 15 (2014) 15981–15993.

[25] G. Vijayakumar, R. Tamilarasan, M. Dharmendirakumar, Adsorption, kinetic, equilibrium and thermodynamic studies on the removal of basic dye Rhodamine-B from aqueous solution by the use of natural adsorbent perlite, J. Mater. Environ. Sci., 3 (2012) 157–170.

[26] M. Nasrollahzadeh, F. Babaei, P. Fakhri, B. Jaleh, Synthesis, characterization, structural, optical properties and catalytic activity of reduced graphene oxide/copper nanocomposites, RSC Adv., 5 (2015) 10782–10789.

[27] T.J. Bandosz, Activated Carbon Surfaces in Environmental Remediation, Academic Press, United States - Cambridge - Massachusetts, 2006.

[28] T.D. Kühne, M. Krack, M. Parrinello, Static and dynamical properties of liquid water from first principles by a novel Car–Parrinello-like approach, J. Chem. Theory Comput., 5 (2009) 235–241.

[29] J.P. Perdew, K. Burke, M. Ernzerhof, Generalized gradient approximation made simple, Phys. Rev. Lett., 77 (1996) 3865–3868.

[30] A. Dal Corso, Pseudopotentials periodic table: from H to Pu, Comput. Mater. Sci., 95 (2014) 337–350.

[31] S. Grimme, Do special noncovalent π–π stacking interactions really exist? Angew. Chem. Int. Ed., 47 (2008) 3430–3434.

[32] P. Giannozzi, S. Baroni, N. Bonini, M. Calandra, R. Car, C. Cavazzoni, D. Ceresoli, G.L. Chiarotti, M. Cococcioni, I. Dabo, A. Dal Corso, S. de Gironcoli, S. Fabris, G. Fratesi, R. Gebauer, U. Gerstmann, C. Gougoussis, A. Kokalj, M. Lazzeri, L. Martin-Samos, N. Marzari, F. Mauri, R. Mazzarello, S. Paolini, A. Pasquarello, L. Paulatto, C. Sbraccia, S. Scandolo, G. Sclauzero, A.P. Seitsonen, A. Smogunov, P. Umari, R.M. Wentzcovitch, QUANTUM ESPRESSO: a modular and open-source software project for quantum simulations of materials, J. Phys.: Condens. Mater., 21 (2009) 395502 (1–19), doi: 10.1088/0953-8984/21/39/395502.

[33] E.R. Johnson, S. Keinan, P.M. Sánchez, J.C. García, A.J. Cohen, W. Yang, Revealing non-covalent interactions, J. Am. Chem. Soc., 132 (2010) 6498–6506.

[34] H.N. Tran, S.J. You, A. Hosseini-Bandegharaei, H.P. Chao, Mistakes and inconsistencies regarding adsorption of contaminants from aqueous solutions: a critical review, Water Res., 120 (2017) 88–116.

[35] X. Xiao, R. Hao, M. Liang, X. Zuo, J. Nan, L. Li, W. Zhang, One-pot solvothermal synthesis of three-dimensional (3D) BiOI/BiOCl composites with enhanced visible-light photocatalytic activities for the degradation of bisphenol-A, J. Hazard. Mater., 233–234 (2012) 122–130.

[36] L. Zhao, X. Cao, W. Zheng, Q. Wang, F. Yang, Endogenous minerals have influences on surface electrochemistry and ion exchange properties of biochar, Chemosphere, 136 (2015) 133–139.

[37] F. Liu, Y. Dai, S. Zhang, J. Li, C. Zhao, Y. Wang, C. Liu, J. Sun, Modification and application of mesoporous carbon adsorbent for removal of endocrine disruptor bisphenol A in aqueous solutions, J. Mater. Sci., 53 (2017) 2337–2350.

[38] M. Thommes, K. Kaneko, A.V. Neimark, J.P. Olivier, F. Rodriguez-Reinoso, J. Rouquerol, K.S.W. Sing, Physisorption of gases, with special reference to the evaluation of surface area and pore size distribution (IUPAC Technical Report), Pure Appl. Chem., 87 (2015) 1051–1069.

[39] C.T. Hsieh, H. Teng, Influence of mesopore volume and adsorbate size on adsorption capacities of activated carbons in aqueous solutions, Carbon, 38 (2000) 863–869.

[40] J. Goscianska, M. Marciniak, R. Pietrzak, Ordered mesoporous carbons modified with cerium as effective adsorbents for azo dyes removal, Sep. Purif. Technol., 154 (2015) 236–245.

[41] I. Bautista-Toledo, M.A. Ferro-García, J. Rivera-Utrilla, C. Moreno-Castilla, F.J.V. Fernández, Bisphenol-A removal from water by activated carbon. Effects of carbon characteristics and solution chemistry, Environ. Sci. Technol., 39 (2005) 6246–6250.

[42] D.J.K. Robert Silverstein, F.X. Webster, Spectrometric Identification of Organic Compounds, 7th ed., Wiley, United States - Hoboken - New Jersey, 2005.

[43] R.D. Kumar, G.K. Kannan, K. Kadirvelu, Populus tree wood: a noble bioresource from western Himalayas for the development of various carbon types for the effective application in environment protection, i.e., phenol adsorption from wastewater, J. Biorem. Biodegrad., 8 (2017) 1–11.

[44] H. Tang, M. Wang, T. Lu, L. Pan, Porous carbon spheres as anode materials for sodium-ion batteries with high capacity and long cycling life, Ceram. Int., 43 (2017) 4475–4482.

[45] M.A.A. Junior, J.T. Matsushima, M.C. Rezende, E.S. Gonçalves, J.S. Marcuzzo, M.R. Baldan, Production and characterization of activated carbon fiber from textile PAN fiber, J. Aerosp. Technol. Manage., 9 (2017) 423–430.

[46] S. Schimmelpfennig, B. Glaser, One step forward toward characterization: some important material properties to distinguish biochars, J. Environ. Qual., 41 (2011) 1–13.

[47] J. Valença, P.R. Olivato, D.N. Rodrigues, P.R. Batista, L.C. Ducati, M. Dal Colle, Conformational analysis and electronic interactions of some 2-[2'-(4'-sustituted-phenylsulfanyl)-acetyl]-5-substituted furans and 2-[2'-(phenylselanyl)-acetyl]-5-methylfuran, J. Mol. Struct., 1225 (2021) 129088 (1–15), doi: 10.1016/j.molstruc.2020.129088.

[48] S. Jafari, B. Yahyaei, E.K. Nejman, M. Sillanpää, The influence of carbonization temperature on the modification of TiO_2 in the removal of methyl orange from aqueous solution by adsorption, Desal. Water Treat., 57 (2016) 18825–18835.

[49] R. Wirasnita, T. Hadibarata, A.R.M. Yusoff, Z. Yusop, Removal of bisphenol A from aqueous solution by activated carbon derived from oil palm empty fruit bunch, Water Air Soil Pollut., 225 (2014) 1–12.

[50] C.R.A. Machado, E.M. Saggioro, Y.G.L. Silva, L.P.S. Pereira, J.C. Campos, Avaliação da adsorção de fenol e bisfenol A em carvões ativados comerciais de diferentes matrizes carbonáceas, Rev. Ambient. Água, 10 (2015) 915–927.

[51] Y.S. Ho, G. McKay, Pseudo-second-order model for sorption processes, Process Biochem., 34 (1999) 451–465.

[52] Y. Dong, D. Wu, X. Chen, Y. Lin, Adsorption of bisphenol A from water by surfactant-modified zeolite, J. Colloid Interface Sci., 348 (2010) 585–590.

[53] J. Xu, L. Wang, Y. Zhu, Decontamination of bisphenol A from aqueous solution by graphene adsorption, Langmuir, 28 (2012) 8418–8425.

[54] A.O. Ifelebuegu, J.E. Ukpebor, C.C. Obidiegwu, B.C. Kwofi, Comparative potential of black tea leaves waste to granular activated carbon in adsorption of endocrine disrupting compounds from aqueous solution, Global J. Environ. Sci. Manage., 1 (2015) 205–214.

[55] P.N. Diagboya, B.I. Olu-Owolabi, K.O. Adebowale, Microscale scavenging of pentachlorophenol in water using amine and tripolyphosphate-grafted SBA-15 silica: batch and modeling studies, J. Environ. Manage., 146 (2014) 42–49.

[56] B.I. Olu-Owolabi, P.N. Diagboya, K.O. Adebowale, Evaluation of pyrene sorption-desorption on tropical soils, J. Environ. Manage., 137 (2014) 1–9.

[57] K.G. Akpomie, F.A. Dawodu, K.O. Adebowale, Mechanism on the sorption of heavy metals from binary-solution by a low cost montmorillonite and its desorption potential, Alexandria Eng. J., 54 (2015) 757–767.

[58] A.A. Alghamdi, A.B. Al-Odayni, W.S. Saeed, A. Al-Kahtani, F.A. Alharthi, T. Aouak, Efficient adsorption of Lead(II) from aqueous phase solutions using polypyrrole-based activated carbon, Materials, 12 (2019) 1–16.

[59] N.A.A. Nazri, R.S. Azis, H.C. Man, A.H. Shaari, N.M. Saiden, I. Ismail, Equilibrium studies and dynamic behaviour of cadmium adsorption by magnetite nanoparticles extracted from mill scales waste, Desal. Water Treat., 171 (2019) 115–131.

[60] W.T. Tsai, C.W. Lai, T.Y. Su, Adsorption of bisphenol-A from aqueous solution onto minerals and carbon adsorbents, J. Hazard. Mater., 134 (2006) 169–175.

[61] M.A.S.D. Barros, P.A. Arroyo, E.A. Silva, General Aspects of Aqueous Sorption Process in Fixed Beds, H. Nakajima, Ed., Advances in Sustainable Energy and Environment Oriented Numerical Modeling, Intech, 2013, pp. 361–386. Available at: https://www.intechopen.com/books/mass-transfer-advances-in-sustainable-energy-and-environment-oriented-numerical-modeling/general-aspects-of-aqueous-sorption-process-in-fixed-beds

[62] N. Özbay, A.S. Yargiç, R.Z. Yarbay-Sahin, E. Önal, Full factorial experimental design analysis of reactive dye removal by carbon adsorption, J. Chem., 2013 (2013) 1–13.

[63] S. Rangabhashiyam, N. Anu, G. Nangagopal, N. Selvaraju, A novel approach of the modified BET isotherm towards continuous column study, J. Sci. Ind. Res., 73 (2014) 489–494.

[64] Z. Gong, S. Li, J. Ma, X. Zhang, Synthesis of recyclable powdered activated carbon with temperature responsive polymer for bisphenol A removal, Sep. Purif. Technol., 157 (2016) 131–140.

[65] S. Bele, V. Samanidou, E. Deliyanni, Effect of the reduction degree of graphene oxide on the adsorption of bisphenol A, Chem. Eng. Res. Des., 109 (2016) 573–585.

[66] T. Phatthanakittiphong, G.T. Seo, Characteristic evaluation of graphene oxide for bisphenol A adsorption in aqueous solution, Nanomaterials, 128 (2016) 1–17.

[67] Í.F.T. Souza, D.F.S. Petri, β-cyclodextrin hydroxypropyl methylcellulose hydrogels for bisphenol A adsorption, J. Mol. Liq., 266 (2018) 640–648.

[68] F. Wang, X. Lu, W. Peng, Y. Deng, T. Zhang, Y. Hu, X.Y. Li, Sorption behavior of bisphenol A and triclosan by graphene: comparison with activated carbon, ACS Omega, 2 (2017) 5378–5384.
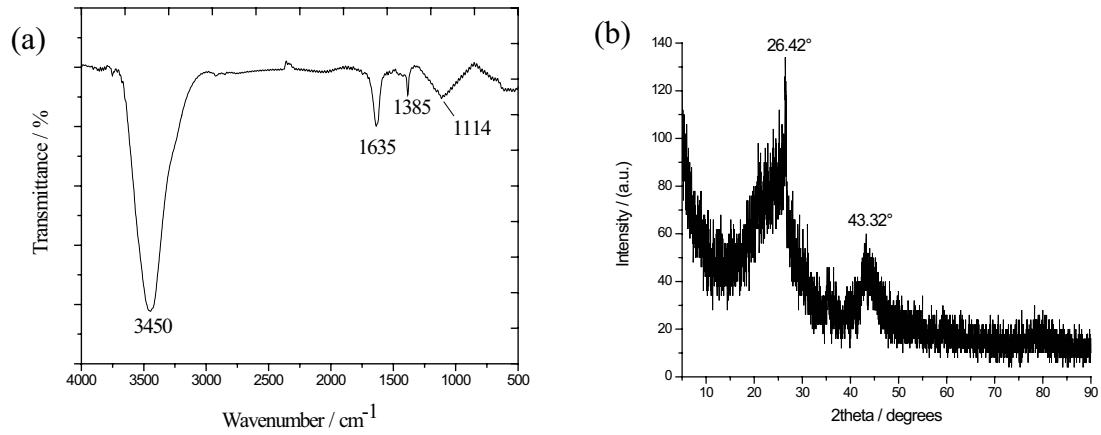
Supplementary information

Fig. S1. Fourier transform infrared spectroscopy (FTIR) analysis (a), and X-ray diffraction (b) of PAC.
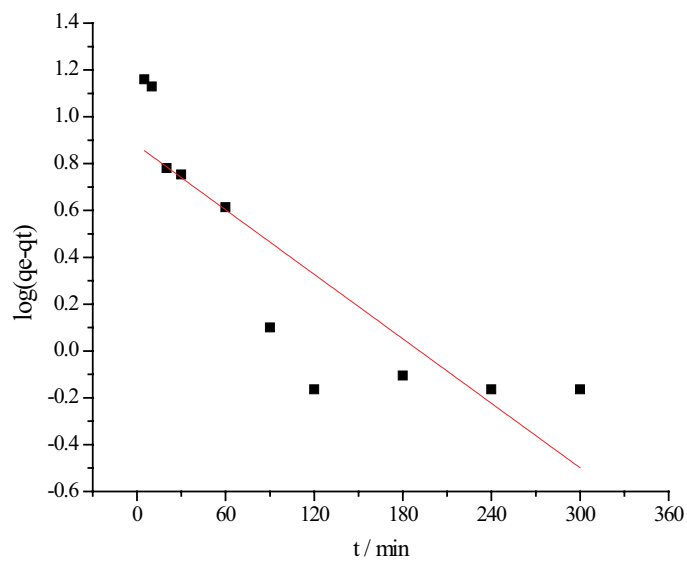

Fig. S2. Kinetic study of bisphenol A removal by PAC evaluated by pseudo-first-order model (0.01 g of adsorbent; 25 mL of 100 mg/L BPA solution; pH 7; 200 rpm; 25°C ± 2°C).